AIAA JOURNAL
Vol. 35, No. 4, April 1997

Time-Resolved Wave Front Measurements Through a Compressible Free Shear Layer

Ronald J. Hugo* and Eric J. Jumper†
University of Notre Dame, Notre Dame, Indiana 46556
and
George Havener‡ and Chip Stepanek§
Arnold Engineering Development Center, Arnold Air Force Base, Tennessee 37389

Time series of spatially resolved, aberrated wave fronts distorted by propagation through a compressible shear layer are presented. These wave fronts were measured using the small-aperture beam technique (SABT) applied to the compressible free shear layer facility at Arnold Engineering Development Center. Two viewing stations were investigated at the facility, the first directly downstream of the compressible shear layer's splitter plate and the second at a location 48.3 cm downstream of the first station. The first station was found to have optically active structures of approximately 2.5 cm in spatial extent, convecting at approximately 160 m/s, and inducing rms aberrations on the order of 0.06 waves. The second station had optically active structures approximately 5 cm in size, also convecting at approximately 160 m/s, and causing distortions on the order of 0.17 waves. The SABT was shown to be an effective means of measuring high-bandwidth optical wave fronts in a far from ideal laboratory setting.

I. Introduction

THE study of optical transmission characteristics through compressible shear layers is usually performed for two distinct reasons: first, to quantify some characteristic of the compressible shear layer's fluid mechanics and, second, to quantify the optical degradation imposed by the shear layer on the optical wave front. The engineering significance of the first case is to study mixing layer development for flow research purposes, whereas the significance of the second case is to quantify the flowfield's aberrating effects on the transmission/receiving characteristics of an optical system needing to transmit through the compressible shear layer. Although the objectives are different and, in general, the specific information sought is different, it is clear that the two purposes are interrelated as an aberrated optical signal is caused by the variant index-of-refraction field generated by the convecting flowfield structures. In the case of airborne optical platforms, that might include airborne imaging or tracking systems or, of more recent interest, airborne laser weapon systems; the aberrating influence of flight Mach number compressible shear layers can be a major driver in the overall system design. The association of the study of the optical transmission quality of free and wall-bounded shear layers with airborne optical systems is referred to as aero-optics.

Optical aberration of a wave front is usually quantified as root-mean-square optical path difference (OPD_{rms}), in units of length, and provides a statistical description of how much a planar optical wave front leads and/or lags its mean wave front position, averaged over the viewing aperture, after emerging from the aberrating flow. The aberration may also be quantified in terms of waves, which is the magnitude of the OPD_{rms} divided by the wavelength of the optical signal λ. Once the wave front error is known in waves, an estimate of the system performance degradation can be made. Such degradation is often quantified by S, the Strehl ratio,[1] which is a ratio of the peak intensity of the so-called far-field pattern formed by the optical beam with aberrations present, I, to the peak intensity for the unaberrated beam (i.e., the diffraction-limited case), I_0. The Strehl ratio is usually estimated using the large-aperture approximation,[2] which assumes that the spatial scale of the aberrations are both random and small compared to the dimensions of the aperture:

$$S = \exp\left(-\left[2\pi \frac{\mathrm{OPD}_{\mathrm{rms}}}{\lambda} \right]^2 \right) \tag{1}$$

From Eq. (1) it can be seen that 0.1 waves of wave front distortion leads to a Strehl ratio of 0.674. In the case of laser weapon systems where the intensity on target is the damage mechanism, this means a 33% loss in effectiveness. In the case of organized structure on the wave front, the large-aperture approximation has been shown to underestimate the reduction in Strehl ratio.[3] Clearly, detailed knowledge of the instant-to-instant aberrating environment has a direct impact on the laser power sizing requirements of such systems that in turn directly affect the overall airborne platform.

One of the first aero-optical investigations was performed by Stine and Winovich[4] in 1956, where the Strehl ratio for transmission through a compressible wall-bounded turbulent mixing layer was measured. Advances in technology have enabled more recent studies to quantify more detail concerning the optical wave front distortion. As an example, Trolinger[5] used pulsed holographic interferometry to measure discrete snapshots of the optical wave front for transmission through aircraft turrets at high-subsonic-flow velocities. Although rich in the amount of spatial data provided, the holographic interferograms were only snapshots of the flowfield and as such were unable to examine the time evolution of the flowfield-induced aberration. Improvements in Shack–Hartmann sensing technology,[6,7] most notably in terms of faster charge-coupled-device array and line-scan cameras, as well as in microlens fabrication techniques, has led to the case where one-dimensional optical wave fronts can be measured at rates of up to 5 kHz (Refs. 8 and 9). The current investigation uses a wave front sensing technique that is a derivative of the Shack–Hartmann sensor; details of the technique are given in a later section.

The investigation presented in this paper was performed in the Acoustic Research Tunnel (ART) located at Arnold Engineering Development Center. The ART facility was modified to produce a compressible shear layer with optical access designed for the purpose of performing aero-optical investigations. The compressible shear layer simulates the shear layer that might be produced by a

Presented as Paper 95-1979 at the AIAA 26th Plasmadynamics and Lasers Conference, San Diego, CA, June 19–20, 1995; received Sept. 6, 1995; revision received Sept. 20, 1996; accepted for publication Dec. 23, 1996.

*Research Coordinator, Department of Aerospace and Mechanical Engineering, Hessert Center for Aerospace Research. Member AIAA.
†Associate Professor, Department of Aerospace and Mechanical Engineering, Hessert Center for Aerospace Research. Associate Fellow AIAA.
‡Principal Engineer, Calspan Corporation/Arnold Engineering Development Center Operations; currently Associate Professor, Department of Aeronautics, U.S. Air Force Academy, CO 80840. Fellow AIAA.
§Senior Engineer, Calspan Corporation/Arnold Engineering Development Center Operations. Member AIAA.

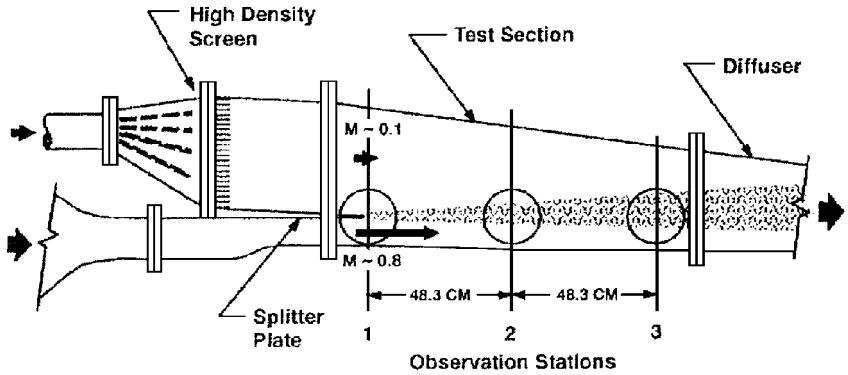

Fig. 1 Schematic of ART facility, from Ref. 10.

transonic-aircraft slip stream flowing past an optical viewing port in the side of the fuselage. A detailed description of the facility can be found in Ref. 10. The shear layer is produced by two uniform airstreams with nominal Mach numbers of 0.8 and 0.1. For the tests reported here, the unit Reynolds numbers for the fast and slow streams were 12.7 and 1.4×10^6/m, respectively. Each stream had the same total temperature, which was approximately the daily atmospheric temperature (27°C, nominally), and the static pressure across the shear layer was constant and equal to stream-matched static pressures of about 0.6 atm (Ref. 10). A schematic of the ART facility is shown in Fig. 1.

The ART facility was designed with three observation windows successively downstream from one another. Each observation station consisted of a total of four windows, two for viewing in the direction of the span of the compressible shear layer (as in the case shown in Fig. 1), and two for viewing in a direction normal to the span of the compressible shear layer. The latter viewing direction involves the scenario most often encountered in a typical aero-optical configuration (viewing through the compressible shear layer over the open cavity of an atmospheric flight vehicle, for example). The original design of the ART facility, as described by Havener and Heltsley,[10] was to use both holographic interferometry and particle image velocimetry simultaneously in order to investigate the flowfield's velocity dynamics and its relation to optical transmission characteristics; however, due to a poor signal-to-noise ratio, Havener and Heltsley were forced to conclude that holographic interferometry could not be used as an appropriate aero-optical diagnostic for the facility.

Instead, a newly developed, time-resolved, one-dimensional wave front sensor, the small aperture beam technique (SABT) sensor,[11,12] was applied to the problem. The results of the application of the SABT sensor to the measurement of aberrations for optical propagation through the ART facility compressible shear layer are reported here. Prior to this application, the SABT wave front sensor had only been applied to an idealized laboratory setting where there were few mechanical vibrations, optical viewing was not restricted by windows, and the flowfield velocities (on the order of 7 m/s) led to frequencies below 5 kHz. The ART facility, on the other hand, presented a difficult flowfield in which to measure the optical aberrations due to the need to view through optical windows, which were inherently coupled with large facility vibrations, and due to the high-flowfield velocities (on the order of 300 m/s) that lead to flowfield frequencies in excess of 30 kHz. To our knowledge, a measurement of time-resolved optical wave fronts for transmission through a compressible free shear layer have never been previously made. This paper presents the application of the SABT to the ART facility, and in the process will discuss the problems encountered, solutions found, and results obtained.

II. Fundamentals of the SABT

As mentioned in the Introduction, the SABT is a method of measuring optical wave fronts at relatively high temporal bandwidth (cf. Refs. 11–13). This bandwidth is high enough to capture a time series of the wave front that resolves the instant-to-instant time evolution of the optical aberrations imposed by structures associated with shear flows well into the compressible regime. The SABT consists of monitoring the off-axis position of multiple small-aperture ($\approx$1 mm) probe beams that traverse an optically aberrating flowfield in a direction normal to the mean convection velocity. Knowing the distance that the probe beam travels between the optically aberrating medium and the location where the off-axis position is monitored, the off-axis angle θ of the emerging probe beam (beam jitter) as a function of time can be directly computed. Through Huygens' principle,[14] the off-axis angle of the emerging beam is known to be equal to the local spatial derivative of the optical wave front at the location of the small-aperture beam's transmission. This is the principle on which Shack–Hartmann wave front sensing is based.[6]

The SABT performs in much the same manner as the Shack–Hartmann wave front sensor (SHWS); however, unlike the SHWS, the SABT takes advantage of the fact that the optically aberrating flowfield is convecting. This idea was first exploited by Malley et al.[15] in the invention of an instrument that used the off-axis time history of a single small-aperture probe beam along with the flowfield's mean convection velocity to compute the statistical $\mathrm{OPD}_{\mathrm{rms}}$ at the small-aperture probe beam's flowfield location. The SABT builds on the ideas of Malley et al. and extends them by using multiple probe beams, allowing for the construction of time-resolved and large- (relative to the small-aperture beam itself) aperture optical wave fronts with a fewer number of sensors than the traditional SHWS. This reduced requirement on the number of sensors necessary to construct a given optical wave front reduces the demands on the data-acquisition system, leading to the case where high temporal bandwidth can be achieved. Although the SABT is, at present, only able to construct wave fronts in the flow direction, many flowfields of aero-optical interest, such as the one reported on here, are essentially two dimensional over large regions where optical propagation would take place. As such, the one-dimensional wave front can be generalized to the cross-stream direction, thereby rendering a full two-dimensional wave front.

The fundamental equations behind the SABT can be derived by starting with the basic equation on which the SHWS is based[6]:

$$\left.\frac{\mathrm{dOPL}(t,x)}{\mathrm{d}x}\right|_{x=0} = \theta(t, x=0) \tag{2}$$

where OPL is the optical-path length and θ is the off-axis angle of the small-aperture probe beam, both at time t and spatial location $x = 0$. Multiplying this equation by the instantaneous convection velocity results in

$$\left.\frac{\mathrm{dOPL}(t,x)}{\mathrm{d}x}\right|_{x=0} \frac{\mathrm{d}x}{\mathrm{d}t} = \theta(t, x=0)U_c \tag{3}$$

Doing this implicitly assumes that all of the optically active medium along the OPL convects at the same velocity U_c. Integrating this equation with respect to time yields

$$\mathrm{OPL}(t, x=0) = \int_{t_0}^{t} \theta(t, x=0)U_c \,\mathrm{d}t + \mathrm{OPL}(t_0, x=0) \tag{4}$$

This is an equation for the OPL at the location of the small-aperture beam ($x = 0$) as a function of time. The goal is to obtain the optical wave front both as a function of space (across the aperture) and

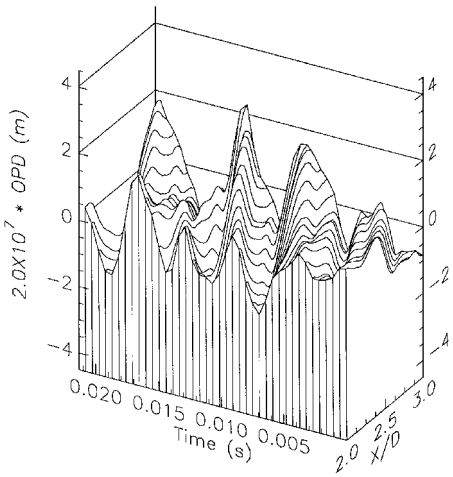

Fig. 2 Space–time representation of reconstructed OPDs for experimental two-dimensional heated jet flowfield, from Ref. 12.

time. This can be computed using the frozen flow assumption and the following equation:

$$x = \_U_c(t \_ t*) \tag{5}$$

where $t*$ refers to the instant in time at which the spatial OPL is desired. Equations (4) and (5) compose the basic theory on which the SABT is based. Application of these equations requires special care in the evaluation of the instantaneous convection velocity and in the determination the flowfield-evolution rate to assess the applicability of the frozen flow assumption (cf. Refs. 11–13).

An example of a time series of one-dimensional wave fronts acquired using the SABT over an aperture equal to one nozzle width over a time period roughly equal to four structure-clearing times for optical propagation through a two-dimensional heated jet is shown in Fig. 2 (Ref. 12); these wave fronts are presented in a space-time waterfall-plot format. The data presented in Fig. 2 were acquired at two nozzle widths downstream of the jet nozzle exit plane. The individual peaks and valleys in the waterfall plot represent the motion of large-scale coherent structures through the viewing aperture ($2.0 < X/D < 3.0$). Similar constructions for the data from the ART facility will be presented in the same waterfall-plot format in a later section.

III. Applying SABT to the ART Facility

The ART flowfield facility along with the SABT hardware can be seen in Fig. 3, and a schematic of the optical-bench layout for the experiment is shown in Fig. 4. In the configuration shown, the optical bench was positioned for measurement at station 2. In the background of the picture is a low-power He–Ne laser beam ($\approx$1 mW), which is directed through a two-lens telescoping system and then toward a beam-splitter device. The purpose of the beam-splitter device is to split the one He–Ne beam into multiple probe beams, each spaced a variable but equal distance δ apart. Only two probe beams were used in the experiment, with the first probe beam fixed at a given spatial location and the second probe beam traversed in the downstream direction.

After leaving the beam-splitter device, the two probe beams were reflected off of the first directing mirror (one 90-deg z-to-y axis turn; cf. Fig. 4), transmitted upward through the window at the bottom of station 2, then through the shear layer, and then out through the window at the top of station 2. The beams were then reflected off of the two return mirrors (two 90-deg turns, the first a y to z and the second a z to y) and then traveled back (external of the flowfield facility) to the optical bench where they encountered the second directing mirror (one 90-deg y-to-z axis turn). The beams, traveling horizontally, were then reflected through a 90-deg z-to-x axis turn and separated before impinging on the position-sensing lateral-effect detectors [United Detector Technologies (UDT) model SC-10D]. The signal from one of the lateral-effect detectors was amplified using two UDT model 301 30-kHz amplifiers, whereas

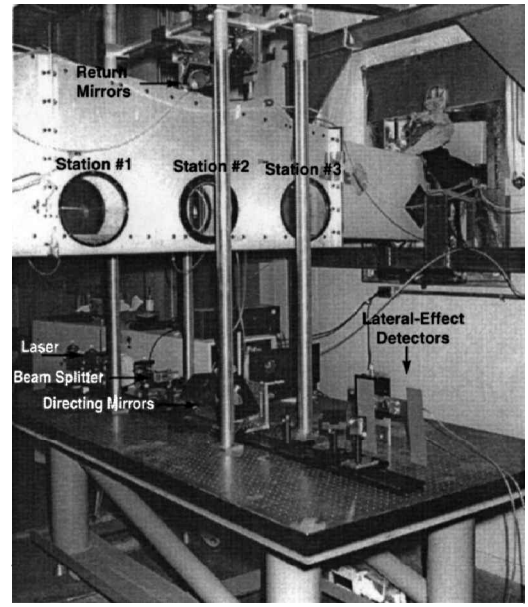

Fig. 3 ART facility with SABT equipment on optical bench.

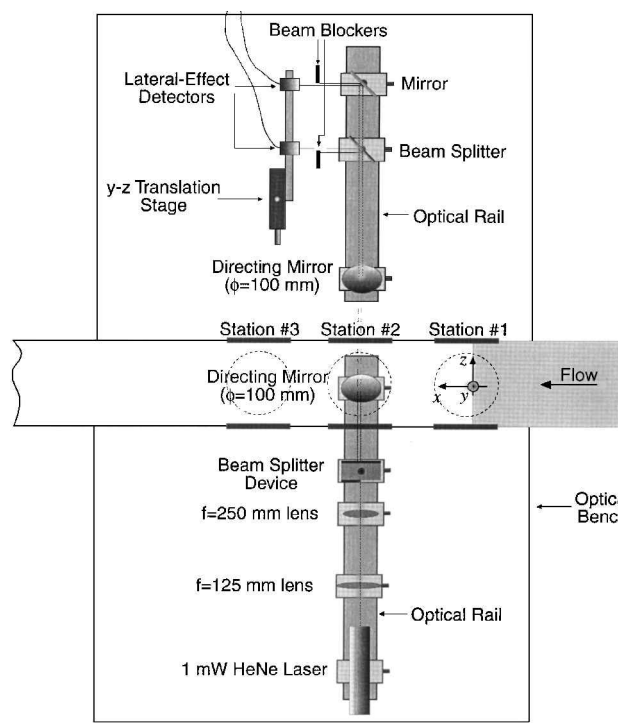

Fig. 4 Top view of optical bench layout.

the signal from the second lateral-effect detector was amplified using an amplifier constructed at Notre Dame (in-house amplifier).

During the experiment, aero-optically aberrated wave fronts were measured at both stations 1 and 2. Data from station 1 were acquired with the first probe beam fixed spatially in the upstream position, while the second probe beam was traversed in the downstream direction in increments of 0.3 cm up to a separation distance of 5.1 cm. Data from station 2 were acquired in a similar manner; however, in this case the second probe beam was traversed in the downstream direction in increments of 0.6 cm up to a separation distance of 5.7 cm. At station 1, six blocks of 4000 data points were acquired at 75 kHz for each probe-beam spacing combination, while a total of five blocks of 4000 data points at 75 kHz were acquired from station 2 for each probe-beam spacing combination. Facility vibrations were assessed by placing accelerometers by the two windows at the bottom of the tunnel through which the probe beams transmitted (one accelerometer per window). The accelerometer signals were acquired at 100 kHz.

Using several techniques detailed in Ref. 16, the vibration, which imposed a jitter onto the probe-beam signals, was determined to be confined to a frequency band between 8 Hz and 2 kHz. Removal of this vibrational noise was achieved through a postprocessing operation by using a high-pass third-order zero-phase-shift Butterworth filter in MATLAB with a cutoff frequency of 2.5 kHz. Details of this procedure are given in Ref. 16.

IV. SABT Data Analysis

After removing the vibrational noise from the beam-jitter signals, the data were in a state that allowed them to be analyzed using the SABT. This data analysis was conducted in two steps: the first step examined the accuracy issues associated with the application of the SABT to the ART-facility flowfield; the second step processed the acquired beam-jitter signals using the SABT, producing optical wave fronts.

Accuracy Issues

As described in detail in Refs. 12 and 13, accuracy issues were addressed by computing the cross-correlation coefficient functions of the beam-jitter signals for different probe-beam spacings. Stationary and nonstationary (cf. the following and Ref. 17) cross-correlation coefficient functions were used to quantify the flowfield-evolution rates. The stationary cross-correlation coefficient function is evaluated by

$$\rho_{\theta_1\theta_2}(\tau, \delta) = \frac{R_{\theta_1\theta_2}(\tau, \delta)}{\sigma_{\theta_1}\sigma_{\theta_2}} = \frac{E[\theta_1(t, x)\theta_2(t + \tau, x + \delta)]}{\sigma_{\theta_1}\sigma_{\theta_2}} \tag{6}$$

where E denotes ensemble averages over many time records, $\theta_1(t, x_1)$ and $\theta_2(t, x_2)$ are the upstream and downstream jitter signals, respectively, and σ_θ is the rms of a particular jitter signal. The nonstationary estimate for the cross-correlation function is evaluated for one single data record (i.e., no ensemble averaging) and over a relatively short period of time (short with respect to the amount of time required to obtain stationarity[17] from the data set). The nonstationary cross-correlation function is given by

$$\hat{R}_{\theta_1\theta_2, t_{\mathrm{OPD}}}(r\Delta t, \delta) = \frac{1}{N}\sum^{N}\theta_1(t_{\mathrm{OPD}} - r\Delta t + i\Delta t, x)\theta_2(t_{\mathrm{OPD}} + i\Delta t, x + \delta) \tag{7}$$

where r represents integer lag numbers ranging from zero up to a predetermined value, N represents the total number of data points used to evaluate the cross-correlation function, and the caret indicates a nonstationary estimate. The maximum value of N was set to cover the convection of approximately two cycles (or structures) in the flow, while the maximum value for r was set at $N/2$.

Stationary cross-correlation coefficient functions were computed for the data from both stations 1 and 2; these results are shown in Figs. 5 and 6, respectively. The data from station 1 showed unusual behavior for the smaller probe-beam spacings in that the expected decay of the maximum value of the cross-correlation coefficient with increasing probe-beam spacing decreased prematurely for $\delta = 1.0$ cm. Otherwise, the curves for larger probe-beam spacings at station 1 and all of the curves at station 2 looked as would be expected; that is, the maximum value of the cross-correlation coefficient decreased with increasing probe-beam spacing and the time delay increased, signifying a longer time for the structure to convect over the longer distance. Taking the maximum values from the cross-correlation coefficient curves for each probe-beam spacing and plotting these values as a function of probe-beam spacing results in the flowfield-evolution-rate curve, shown in Fig. 7 (cf. Refs. 12 and 13).

As detailed in Refs. 12 and 13, the flowfield evolution rate curve allows a means for estimating the magnitude of error in the optical wave front constructions. The optical wave front constructions performed for both stations 1 and 2 used the data for a probe-beam spacing of $\delta = 2.5$ cm. With this spacing, the maximum value of the cross-correlation coefficient function was 0.16 for station 1 and 0.30 for station 2. From the error estimate techniques outlined in Refs. 12 and 13, the OPD error was estimated to be on the order of 18% for station 1 and 12% for station 2 (based on the peak-to-peak value of the constructed wave front).

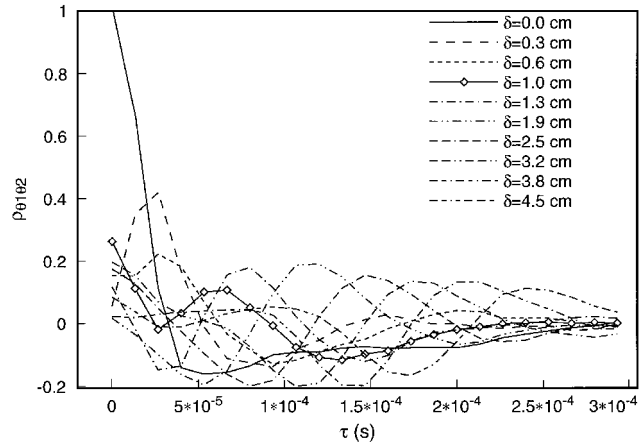

Fig. 5 Stationary cross-correlation coefficient function at station 1.

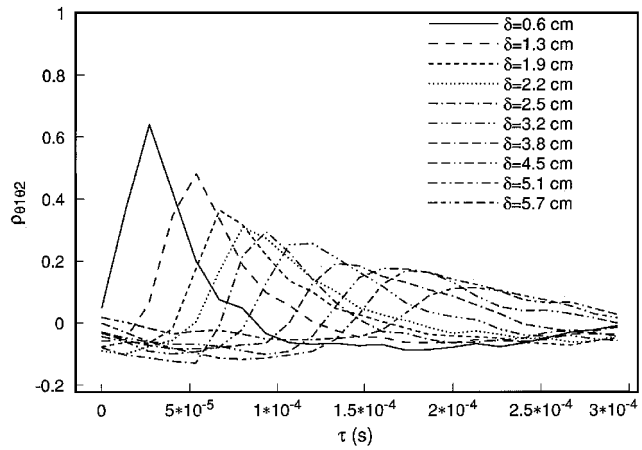

Fig. 6 Stationary cross-correlation coefficient function at station 2.

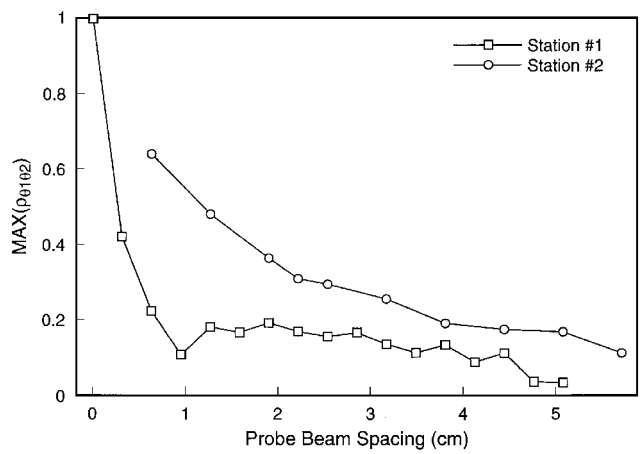

Fig. 7 Flowfield evolution rate.

Extracting more than accuracy estimates for wave front constructions from the stationary cross-correlation coefficient functions should be undertaken with caution. It is tempting, for example, to extract the flowfield aberrating-structure convection velocities by measuring the time delay at which the peak values of the cross-correlation curves occur and dividing this time into the spacing between probe beams. Setting aside uncertainty issues associated with inferring the convection velocity for small probe-beam spacings ($\delta < 1.0$ cm) where the convection time is on the order of the time step between probe-beam samples, applying this method to the stationary cross-correlation coefficient curves at station 1 infer a convection Mach number of approximately 0.43, which is consistent with nonstationary analysis techniques that will be discussed subsequently. A convection Mach number of 0.43 is also consistent with expected structure convection Mach numbers for a free shear

layer with its high-speed stream at Mach 0.8 and its slow-speed stream at Mach 0.1, as is the case here. Use of these stationary cross-correlation curves for station 2 in the same manner as for station 1, however, leads to nonphysical Mach numbers ranging from 0.7 to 0.8. The reasons for these nonphysical inferences is addressed subsequently in the discussion of nonstationary data analysis techniques.

It is also tempting to infer an estimate for the average structure size of the flowfield's optically aberrating structures by examining the stationary cross-correlation coefficient functions. When a second or new maximum value is seen to enter into the cross-correlation coefficient function curve with increased probe-beam spacing, it is known that one entire cycle of the structure has been allowed to pass between probe beams. The inference is that the probe-beam spacing for which this occurs is approximately equal to the average optically active structure's size.

In the case of station 1, obvious second peak entrances are in evidence for $\delta > 1.0$ cm, and structure sizes of approximately 2.5 cm may be inferred; these are consistent with structure sizes measured from wave front constructions, as will be discussed. Such structure size inferences from the station 2 cross-correlation curves are less certain and due to misleading Mach number inferences from these curves, extraction of structure size information should be avoided when using stationary analysis techniques. Because of the care that must be taken when using nonstationary data analysis techniques, inferring both convection Mach number and structure size from stationary data analysis techniques of probe beam data should not, in general, be accepted a priori.

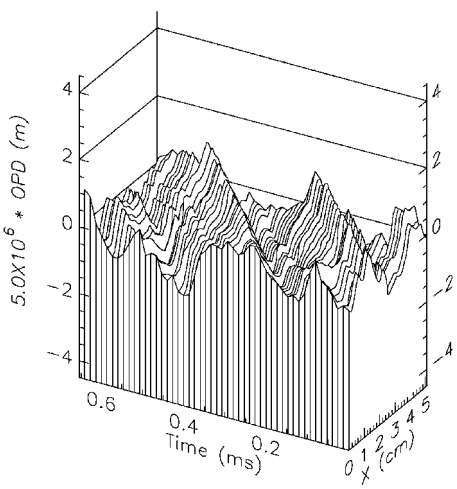

Fig. 8 Station 2 wave front construction (good): δ = 2.5 cm, U = 145.3 m/s, M = 0.427, and $OPD_{rms} = 1.00 \times 10^{-7}$ m $\approx$ 0.158 waves.

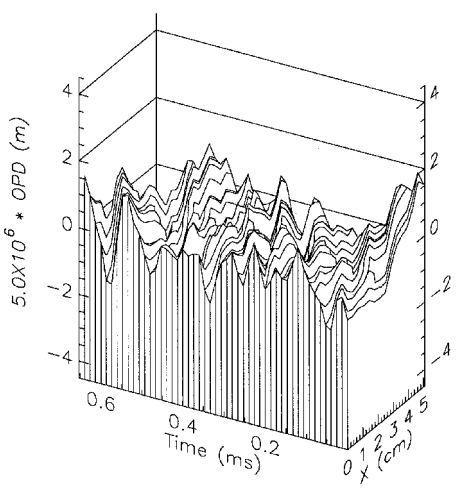

Fig. 9 Station 2 wave front construction (poor): δ = 2.5 cm, U = 263.3 m/s, M = 0.775, and $OPD_{rms} = 9.53 \times 10^{-8}$ m $\approx$ 0.151 waves.

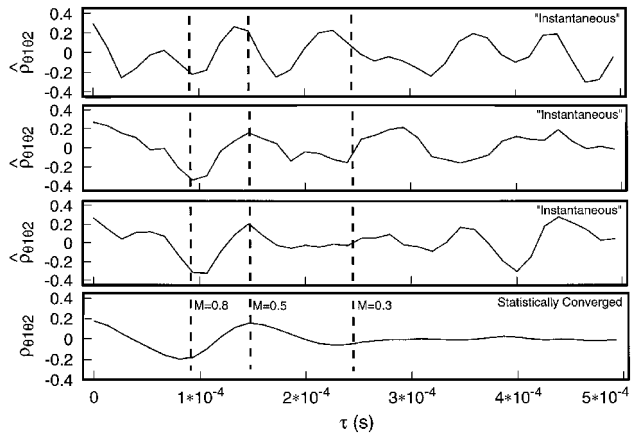

Fig. 10 Cross-correlations station 1.

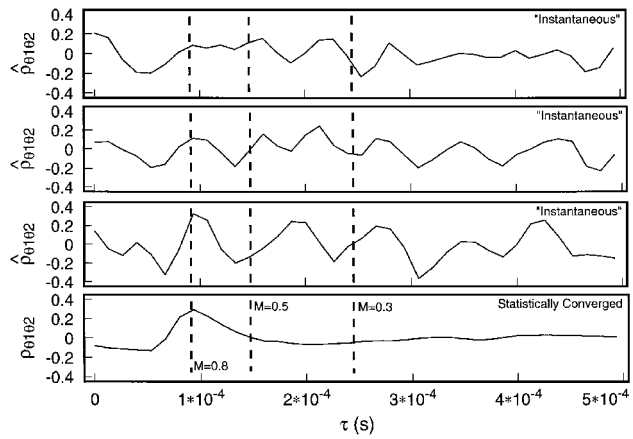

Fig. 11 Cross-correlations station 2.

Optical Wave Front Constructions

The optical wave front constructions can be performed using the ideas presented in Refs. 11–13. Two resulting constructions for station 2 data are shown in the waterfall plots in Figs. 8 and 9. The plot in Fig. 8 shows peaks and valleys moving off in space–time, which were seen before for the heated two-dimensional jet data (Fig. 2); however, the plot in Fig. 9 shows a very poor construction. The mean of the instantaneous Mach numbers that were used for the computation in Fig. 8 was 0.427, whereas the one in Fig. 9 was 0.775. The problem of a high Mach number for station 2 data was also encountered earlier when the Mach number was estimated from the stationary cross-correlation data. In an attempt to further understand the cause of this unrealistically high velocity, the method of velocity estimation was examined and will be discussed next.

In performing the optical wave front constructions, the instantaneous convection velocity was required and, thus, was computed at a given instant in time using nonstationary data analysis techniques. The reason for using nonstationary data analysis techniques is because the true instantaneous convection velocity of the optically aberrating structures varies as a function of time. In performing this instantaneous cross-correlation, data from the passage of approximately two structures were taken from both the upstream and the downstream probe-beam signals and then cross correlated. An example of three instantaneous cross-correlation curves along with the statistically converged cross-correlation curve (i.e., stationary analysis), all at a probe-beam spacing of 2.5 cm, is given for data from stations 1 and 2 in Figs. 10 and 11, respectively. On all of the cross-correlation plots, vertical lines have been drawn at different time delays τ denoting the Mach numbers that would be computed for those time delays with the probe-beam spacing of 2.5 cm.

The instantaneous correlations for station 1, shown in Fig. 10, all show the case where the peaks of the correlation curves are in a region that would yield a Mach number on the order of 0.5. This trend is reflected in the stationary statistically converged correlation curve.

The instantaneous correlations are seen to be periodic in nature with a period on the order of 1.5×10^{-4} s. All three instantaneous correlation curves show one full cycle in the range 0 s $\rightarrow 1.5 \times 10^{-4}$ s, which indicates that the size of the one cycle in the optical aberration (a structure) is approximately the size of the probe-beam spacing, 2.5 cm, in agreement with the earlier discussion on structure sizes. The peak in the correlation curves at $\tau = 1.5 \times 10^{-4}$ s represents the amount of time that it takes a structure to move from the upstream beam to the downstream beam. The smaller magnitude peak evident in the instantaneous correlation curves at a time delay of approximately 7×10^{-5} s would correspond to the front of a structure correlating with the back of a structure or vice versa.

The instantaneous correlations for station 2 shown in Fig. 11, on the other hand, show a different character of periodicity than was seen in the correlations at station 1. The instantaneous correlations are seen to be dominated by cycles of three to four peaks, with the first peak occurring most regularly and at a time delay of 9×10^{-5} s and with the other peaks being less regular and at longer time delays. This peak at a time delay of 9×10^{-5} s, like the 7×10^{-5} s peak for station 1, can be attributed to the correlation of one part of a structure with a different part of the same structure. The fact that the statistically converged correlation curve shows the peak at a time delay of 9×10^{-5} s suggests that the correlation of one part of a structure with a different part of the same structure occurs more frequently (several times per structure) than the correlation between one part of a structure with itself after it has convected downstream. It is believed that this correlation of one part of a structure with a different part of the same structure is what led to the erroneous inference of convection velocity from the stationary cross-correlation curves in Fig. 6.

To remove the nonphysical convection velocity estimates resulting from the correlation of one part of a structure with a different part of the same structure, the tolerances for acceptable Mach numbers or convection velocities in the SABT procedure (cf. Refs. 11–13) were narrowed from the previous range of 0.2 $\rightarrow$ 0.9 to 0.3 $\rightarrow$ 0.6. This restriction served to filter out the erroneous velocity estimates. Figure 12 shows the optical wave fronts constructed using the same beam-jitter data as was used for the waterfall plot in Fig. 9, the only difference being that the construction in Fig. 9 was made using the convection velocity tolerance of 0.2 $\rightarrow$ 0.9, whereas the construction in Fig. 12 was made using the tolerance of 0.3 $\rightarrow$ 0.6. The effect of these new tolerances are reflected by the fact that the mean of the instantaneous Mach numbers is reduced from 0.775 to a more physically realistic 0.421. Also, the characteristic peaks and valleys that would be expected for a convecting structure are seen to be once again present when using the 0.3 $\rightarrow$ 0.6 tolerances.

More constructions are shown for station 2 data in Figs. 13 and 14. The average convection velocity over the time period for the construction, as well as the rms OPD wave front distortion (based on a wavelength of 632.8×10^{-9}), is also given in the figure captions. Of interest is that over certain periods of time, the wave front distortion is noted to be small, with values on the order of 0.1 waves (Fig. 12); whereas at other times the distortions are high and on the order of 0.26 waves (Fig. 13). The size of one optically aberrating structure is seen to be approximately the size of the aperture, 5 cm. Construction data for station 1 are shown in Figs. 15 and 16. Of note is that the rms OPD wave front distortion is much smaller for station 1 than for station 2, with station 1 values being on the order of 0.06 waves.

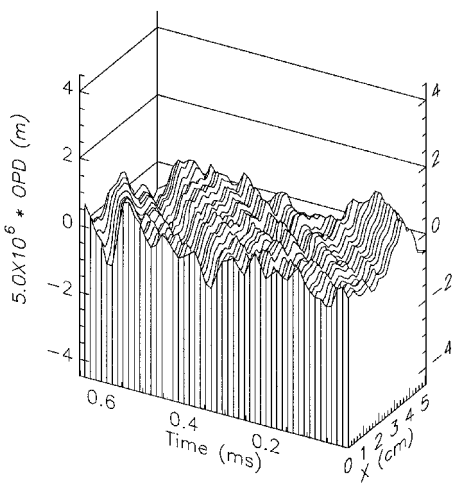

Fig. 12 Station 2 wave front construction (good): δ = 2.5 cm, U = 143.2 m/s, M = 0.421, and $OPD_{rms} = 6.39 \times 10^{-8}$ m $\approx$ 0.101 waves.

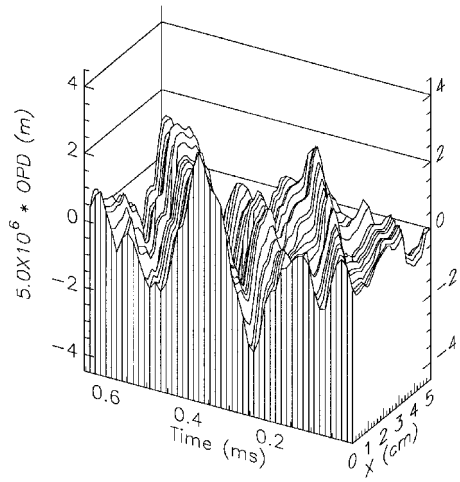

Fig. 13 Station 2 wave front construction: δ = 2.5 cm, U = 190.5 m/s, M = 0.560, and $OPD_{rms} = 1.65 \times 10^{-7}$ m $\approx$ 0.260 waves.

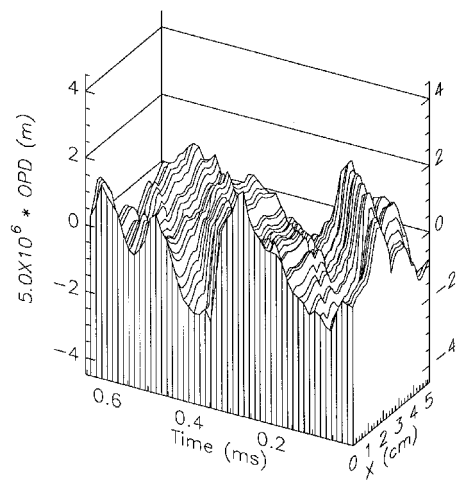

Fig. 14 Station 2 wave front construction: δ = 2.5 cm, U = 173.2 m/s, M = 0.509, and $OPD_{rms} = 1.23 \times 10^{-7}$ m $\approx$ 0.194 waves.

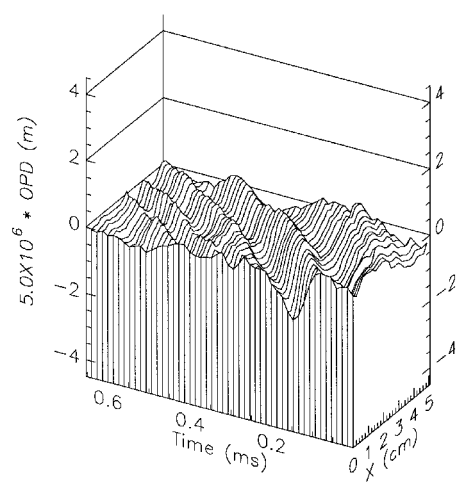

Fig. 15 Station 1 wave front construction: δ = 2.5 cm, U = 133.3 m/s, M = 0.392, and $OPD_{rms} = 5.19 \times 10^{-8}$ m $\approx$ 0.082 waves.

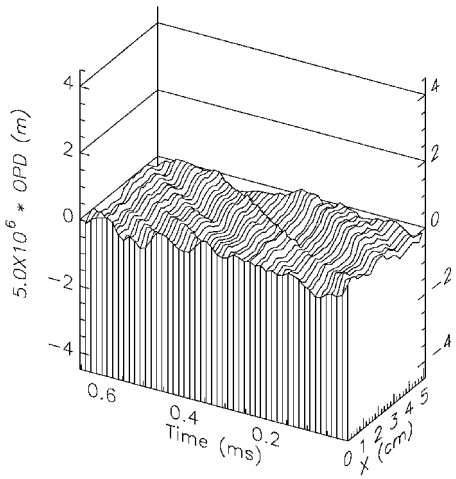

Fig. 16 Station 1 wave front construction: δ = 2.5 cm, U = 105.8 m/s, M = 0.311, and $OPD_{rms} = 2.88 \times 10^{-8}$ m $\approx$ 0.045 waves.

These time series of wave fronts are clearly relevant to airborne optical systems that presently exist and others that are being contemplated, because these systems must contend with performance degradations imposed by optical propagation through compressible shear flows. Until now, performance degradation estimates were forced to rely on statistical measures of the turbulent shear layers that treated the turbulence as random, rather than consisting of the organized structures known to exist in this type of flow.[18]

V. Conclusions

This research represents the first time that continuous time series of spatially resolved wave fronts have been measured; thus, not only can the spatial character of the aero-optically distorted wave fronts be examined in detail, but the nature of their time evolution examined and the resulting system-performance implications computed directly. From the wave front data presented, with accuracies of 18 and 12% of peak-to-peak OPD for stations 1 and 2, respectively, we are able to infer for this compressible shear flow that the optically active structures in the near splitter-plate region (station 1) convect at approximately 160 m/s and that the average rms of the OPD imposed on the wave fronts by these structures was approximately 0.063 waves. Further, the size of an average structure was approximately 2.5 cm, yielding a dominant temporal frequency of approximately 6.5 kHz. At station 2, 50 cm downstream of the splitter plate, the average optical aberration nearly tripled to an rms OPD of approximately 0.17 waves, with maximum rms OPDs found to be as high as 0.26 waves and as low as 0.1 waves. The convection velocities of the aberrating structures remain at approximately 160 m/s; however, the structure sizes over this aperture approximately doubled to 5.0 cm, concomitantly halving the dominant temporal frequency.

The results demonstrate the ability of the SABT wave front sensor to collect wave front data in less than ideal laboratory conditions. The character of these wave fronts is of the same order as those collected in a well-controlled heated-jet facility at Notre Dame (cf. Fig. 2). This suggests that the SABT sensor possesses a high potential for application to a wide range of aero-optical flowfields. Although the intended purpose of the experiment reported here was to examine the spatial and temporal dynamics of the aberrated wave front due to optical propagation through a compressible shear layer, it is clear that the dynamics of the wave front are related to the dynamics of the aberrating fluid structures in the flow. Thus, it is a logical extension of the use of these type wave front data to study shear layer fluid dynamics and mixing in general. In this regard note that unlike optical aberrations imposed by shear layer mixing of two mismatched index-of-refraction streams (like the case of the heated-jet experiments), the aberrating index field caused by the compressible shear layer is due to both the geometric structure of the mixing layer and the thermodynamic processes leading to the variant temperature through the layer. The dynamic wave front data, then, may offer new research opportunities to study these thermodynamic processes as well as other mixing scenarios where the products of the mixing form the variant index field.

Acknowledgment

Effort was sponsored by the U.S. Air Force Office of Scientific Research, Air Force Material Command, U.S. Air Force, under Grant F49620-93-1-0163.

References

[1]Smith, W. J., *Modern Optical Engineering*, McGraw–Hill, New York, 1966, Chap. 3.

[2]Mahajan, V. N., "Strehl Ratios for Primary Aberrations in Terms of Their Aberration Variance," *Journal of the Optical Society of America*, Vol. 73, No. 6, 1983, pp. 860, 861.

[3]Cicchiello, J. M., and Jumper, E. J., "Far-Field Optical Degradation due to Near-Field Transmission Through a Turbulent Heated Jet," *Applied Optics* (to be published).

[4]Stine, H. A., and Winovich, W., "Light Diffusion Through High-Speed Turbulent Boundary Layers," NACA Research Memorandum A56B21, May 1956.

[5]Trolinger, J. D., "Aero-Optical Characterization of Aircraft Optical Turrets by Holography, Interferometry, and Shadowgraph," *Aero-Optical Phenomena*, edited by K. Gilbert and L. J. Otten, Vol. 80, Progress in Astronautics and Aeronautics, AIAA, New York, 1982, pp. 200–217.

[6]Malacara, D., *Optical Shop Testing*, Wiley, New York, 1978, Chap. 6.

[7]Tyson, R. K., *Principles of Adaptive Optics*, Academic, San Diego, CA, 1991.

[8]Neal, D. R., O'Hern, T. J., Torczynski, J. R., Warren, M. E., Shul, R., and McKechnie, T. S., "Wavefront Sensors for Optical Diagnostics in Fluid Mechanics: Application to Heated Flow, Turbulence and Droplet Evaporation," *Optical Diagnostics in Fluid and Thermal Flow*, edited by S. S. Cha and J. D. Trolinger, Vol. 2005, Society of Photo-Optical Instrumentation Engineers (International Society for Optical Engineering), Bellingham, WA, 1993, pp. 194–203.

[9]McMackin, L., Masson, B., Clark, N., Bishop, K., Pierson, R., and Chen, E., "Hartmann Wave Front Sensor Studies of Dynamic Organized Structure in Flowfields," *AIAA Journal*, Vol. 33, No. 11, 1995, pp. 2158–2164.

[10]Havener, G., and Heltsley, F., "Design Aspects and Preliminary Holographic-PIV Measurements for a Subsonic Free Shear Layer Flow Channel," AIAA Paper 94-2550, June 1994.

[11]Jumper, E. J., and Hugo, R. J., "Quantification of Aero-Optical Phase Distortion Using the Small-Aperture Beam Technique," *AIAA Journal*, Vol. 33, No. 11, 1995, pp. 2151–2157.

[12]Hugo, R. J., and Jumper, E. J., "Experimental Measurement of a Time-Varying Optical Path Difference by the Small-Aperture Beam Technique," *Applied Optics*, Vol. 35, No. 22, 1996, pp. 4436–4447.

[13]Hugo, R. J., "Quantifying the Spatio-Temporal Effects of Optically-Active Turbulent Flowfields on a Coherent Optical Wave," Ph.D. Dissertation, Dept. of Aerospace and Mechanical Engineering, Univ. of Notre Dame, IN, April 1995.

[14]Klein, M. V., *Optics*, Wiley, New York, 1970, pp. 18–20.

[15]Malley, M., Sutton, G. W., and Kincheloe, N., "Beam-Jitter Measurements of Turbulent Aero-Optical Path Differences," *Applied Optics*, Vol. 31, No. 22, 1992, pp. 4440–4443.

[16]Hugo, R. J., Jumper, E. J., Havener, G., and Stepanek, S. A., "Time-Resolved, Aero-Optical Measurements of a Wavefront Aberrated by a Compressible Shear Layer," AIAA Paper 95-1979, June 1995.

[17]Bendat, J. S., and Piersol, A. G., *Random Data: Analysis and Measurement Procedures*, 2nd ed., Wiley, New York, 1986, Chap. 12.

[18]Brown, G. L., and Roshko, A., "On Density Effects and Large Structure in Turbulent Mixing Layers," *Journal of Fluid Mechanics*, Vol. 64, Pt. 4, 1974, pp. 775–816.

G. Laufer
Associate Editor